Vol. **1**, **7**. 471-492 (2005)

Revue de Mécanique Appliquée et Théorique

Modeling Pogo instability in rockets

N. El Katchan
Laboratoire de Mécanique, B.P. 2121, Tetouan 93 000, Maroc

L. El Bakkali
Laboratoire de Mécanique, B.P. 2121, Tetouan 93 000, Maroc

F. EL Hassani Bakkali
LGCMS, F.S.T.T., B.P. 416, Tanger 90 000, Maroc

A. Khamlichi
LGCMS, F.S.T.T., B.P. 416, Tanger 90 000, Maroc
Plastex Maroc SA, BP 342 Zone Industrielle, Tanger 90000, Maroc

Résumé

La poussée produite par les moteurs d'un lanceur spatial subit des variations durant la combustion des propergols. Ces variations peuvent entraîner des fluctuations de pression dans les tuyaux d'alimentation des moteurs et provoquer par couplage rétroactif un phénomène de résonance connu sous le nom d'instabilité Pogo. Il en résulte des vibrations transitoires sévères qui risquent d'endommager la charge utile transportée à bord du lanceur. Dans ce travail, un modèle théorique de l'effet Pogo est construit en trois étapes. Premièrement, l'analyse de l'interaction fluide structure dans un réservoir partiellement remplie de propergols liquides est considérée dans le contexte de la méthode des éléments finis. La structure du réservoir est décrite au moyen d'éléments coques axisymétriques obtenus par la formulation classique de Love Kirchhoff. Le liquide supposé incompressible et en écoulement irrotationnel est décrit dans le cadre de la formulation utilisant le potentiel des déplacements par des éléments Q4. L'effet de la gravité sur la surface libre et les conditions de transmissions à l'interface fluide structure ont été aussi pris en compte. Deuxièmement, la caractéristique propulsive des moteurs a été revue et la fonction de transfert des canalisations alimentant le moteur a été établie en admettant l'hypothèse de la propagation des perturbations en ondes planes dans la tuyauterie. Les modes longitudinaux calculés de la fusée sont utilisés finalement via des fonctions de réponse fréquentielles appropriées dans un diagramme en blocs décrivant le processus rétroactif Pogo. Le modèle obtenu, qui permet de relier directement les fluctuations de la poussée induites par les moteurs du lanceur aux fluctuations du débit à l'entrée des moteurs, se révèle être prédictif dans l'analyse des éventualités des instabilités Pogo.

Abstract

Because of thrust fluctuations in space vehicle engines during propellant burn, pressure fluctuations in the engine feedline may appear leading to a resonant coupling phenomenon known as Pogo instability. As an adverse result, severe transient vibrations could occur with possible damage of the transported payloads. In this work, a theoretical modeling of Pogo effect is achieved in three steps. First, analysis of fluid-structure interaction in a propellant tank partially filled with a liquid is considered within the context of the finite element method. The reservoir structure is described by using shell axisymmetric elements resulting from the classical Love Kirchhoff formulation. The fluid is assumed incompressible and irrotational. It is discretized by using the displacement potential formulation with Q4 elements. Gravity effects on the free surface and the transmission conditions at the fluid-shell interface were taken into account. Secondly, the engine thrusting characteristic is reviewed and the engine feedline transfer function is established by assuming the hypothesis of plane wave propagation of

Received 8 July 2003
Revised 11 July 2005

disturbances in the piping system. The computed rocket longitudinal eigenmodes are incorporated finally via appropriate frequency response functions in a bloc diagram describing the Pogo feedback process. The obtained model, which relates directly the thrust fluctuations induced by the rocket engine to fluctuations of the propellant flow rate at the engine inlets, enables straightforward analysis of Pogo instability occurrence.

Key words: Reservoir, Liquid propellant, Elastic shells, Sloshing, Hydro-elasticity, Incompressible fluids, Finite element method, Pogo effect, Vibrations, Stability

Mots clés: Réservoir, Propergols liquides, Coques élastiques, Ballottement, Hydro-élasticité, Fluide incompressible, Méthode des éléments finis, Effet Pogo, Vibrations, Stabilité

1. INTRODUCTION

Pogo is the name given to a dynamic instability phenomenon that can occur during ascent of space vehicles propelled by liquid rocket engines [1].

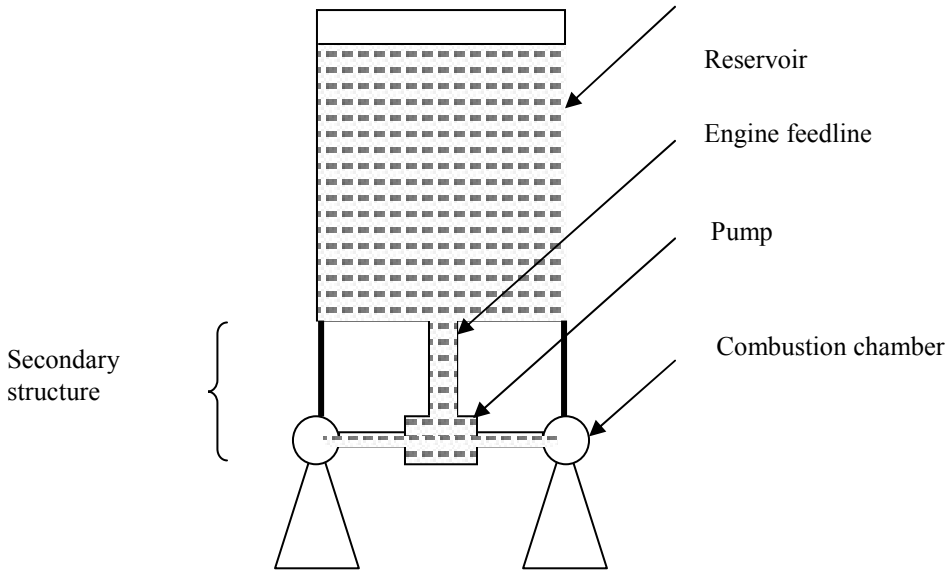

Figure 1: Schematic for the engine reservoir coupling

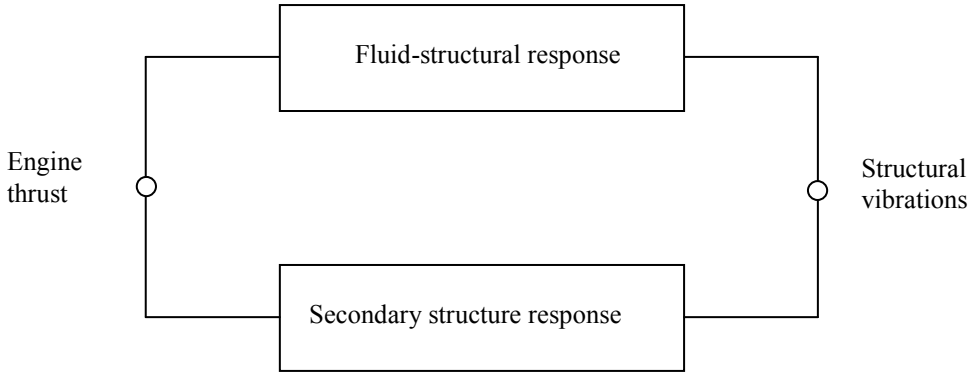

Figure 2: Block diagram of Pogo feedback process

The instability is due to the coupling between structural vibration of the vehicle in one of its normal modes and thrust oscillation of the engines. Pogo occurs most often in the first longitudinal vehicle mode (like a Pogo stick motion).
When the vehicle vibrates longitudinally, the pump and the propellant in the flexible tank undergo oscillatory motions. These two motions produce oscillating flow in the engine piping system including, as shown in the schematic figure 1, the feedline and the pump discharge line. The flow oscillations lead to oscillations in engine thrust and in pressure at the pump inlet, which then excite the vehicle structure. The feedback loop is thereby closed.
This closed-loop can lead to instability if thrust perturbation is in synchronism with structural vibration and if the amplitude and phasing of thrust perturbation are such that sufficient positive work is produced to overcome structural damping and hydraulic losses.
A block diagram of the positive feedback process which can lead to Pogo instability is shown in figure 2. Fluid-structural response is the direct block and the secondary structure response acts like the feedback block.
During first and second liquid stage burn of medium and heavy lift vehicles, severe Pogo has occurred between 5 and 50 Hz. The instability exhibits a slowly varying amplitude, first building to a maximum and then decaying over a period which is in general smaller than 30 s.
Pogo has caused engine shutdowns on two occasions (a Titan Stage I and a Saturn V S-II stage) and has caused intolerable vibration of launch vehicle structure and of payloads.
For these reasons, all the dynamic excitations experienced by a space vehicle during various pre-flight and flight events should be predicted and evaluated. But, it is well known that Pogo excitations could be the dominant dynamic excitations, if they occur [1].
Among the known means that has proven successful in eliminating prior Pogo occurrences and preventing Pogo during the design stage, one finds incorporating gas-charged accumulators at engine inlets [1].
In an attempt to understand more closely Pogo instability mechanisms, we proceed in this work to achieving numerical computation of harmonic hydroelastic vibrations under gravity for an axisymmetric thin shell partially filled by an incompressible fluid. This problem which aims modeling the rocket reservoir has been in the past the subject of various studies. Among these, one can find in [2] the presentation of a variational principle which take into account fluid-structure interaction and in [3] theoretical and numerical studies related to the problem of a fluid contained in a deformable thin shell structure. Bermudez, [4], gives a complete description of a reservoir model based on the finite element method. Implementation issues were discussed and numerical experiments have shown the effectiveness of the method. The sloshing and the elastic modes of an elastic reservoir containing a liquid were computed. These authors have not used however shell geometrical approximation for the reservoir structure since they have worked with the complete field equations of elasticity. Following these approaches, the present analysis is considered within the framework of the linearized theory [2] where the general equations of the coupled fluid-elastic shell correspond to the range of small vibrations. Furthermore, Love Kirchhoff shell deformation theory is used for the reservoir structure. An appropriate variational formulation of the problem is introduced after that. Then adequate approximations of the different terms appearing in the system total energy functional yield the spectral coupled problem to be solved.
Since also combustion of the propellant liquid causes the fluid mass to diminish as function of the flight time, computation of the coupled modes as functions of the fluid depth level is performed. The obtained modes characterize the system evolution from a mechanical point of view and yield explicit frequency response functions between the anchoring points of the rocket engine and the upstream end of the engine feedline.
In section 3 and 4, we present a classical one dimensional modeling generally used for the secondary structure of the rocket. This includes the transfer function between the two ends of the engine feedline,

a simplified model for the pump discharge linking the engine feedline and the combustion chamber and finally an analytical model for the rocket engine. This last gives an explicit relation between the propellant flow rate at the inlet of the combustion chamber and the rocket thrust.
In section 5, all the coupling blocks are considered to build a discrete closed loop model for Pogo effect. Two transfer functions are used: (a) the time varying frequency response function between the anchoring points of the engine and the upstream end of the secondary structure; (b) the transfer function between the upstream end of the engine feedline and the rocket thrust.
In section 6, the Pogo discrete model is used in order to perform parametric studies. It is found that for some specific rocket launching parameters instability may occur.

2. MODELING THE ROCKET RESERVOIR

2.1 Notations

Let Ω_F and Ω_S be the domains occupied by the fluid and the solid, respectively, which are supposed to be bodies of revolution. Let us denote by Γ_F the boundary of the fluid domain and by $n_F = n$ its unit normal vector pointing outwards Ω_F. This boundary is splitted into two parts: the interface between the solid and the fluid Γ_1 and the free surface Γ_2. On the other hand the solid boundary is the union of three parts: the interface Γ_1, Γ_u where the displacement is prescribed and Γ_σ assumed to be free of stresses. Finally $n_S = -n$ denotes the unit outward normal vector along Γ_σ. The other notations used are as follows: u is the fluid displacement vector; v the solid displacement vector; p the pressure; ρ_F the fluid density; ρ_S the solid density; ε the strain tensor and σ the stress tensor. Figure 3 gives a summary of the principal notations used.

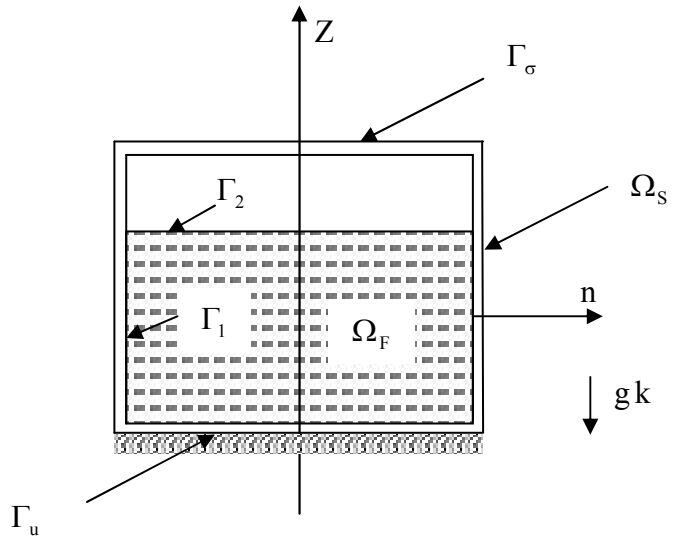

Figure 3: Tank configuration and notations used

2.2 Equations of the coupled problem

The liquid filling the deformable reservoir is assumed to be inviscid and incompressible. The structure is assumed to be a thin elastic shell. Under gravity loads initial displacements and prestresses are produced. Within the scope of this work where only small amplitude motions from this prestressed equilibrium are considered. Let us define the displacement potential φ by

$$p = \omega^2 \rho_F \varphi + p_0 \tag{1}$$

where p_0 is a constant to be determined later on. From the displacement potential the displacement is recovered by: $u = \nabla\varphi$. If the classical linearization procedure [2] is stated one obtains the following eigenvalues problem for the vibration modes of the coupled system and their corresponding angular frequencies ω.

Find $\omega \geq 0$, v, γ and φ, $(v,\gamma,\varphi) \neq (0,0,0)$, such that:

$$\Delta\varphi = 0 \qquad \text{in} \quad \Omega_F, \tag{2}$$

$$\nabla.\sigma(v) + \omega^2 \rho_S v = 0 \qquad \text{in} \quad \Omega_S, \tag{3}$$

$$\varphi_{,n} - v.n = 0 \qquad \text{on} \quad \Gamma_1, \tag{4}$$

$$\sigma(v)n + \omega^2 \rho_F \varphi n + p_0 n - \rho_F g (k.n)(v.n) n = 0 \qquad \text{on} \quad \Gamma_1, \tag{5}$$

$$\varphi_{,n} - \gamma = 0 \qquad \text{on} \quad \Gamma_2, \tag{6}$$

$$\omega^2 \rho_F \varphi + p_0 - \rho_F g \gamma = 0 \qquad \text{on} \quad \Gamma_2, \tag{7}$$

$$\sigma(v)n = f \qquad \text{on} \quad \Gamma_\sigma, \tag{8}$$

$$v = 0 \qquad \text{on} \quad \Gamma_u. \tag{9}$$

where k is the descendant vertical vector, f is a given force per unit surface area and the new variable, $\gamma = u.n$ defined on Γ_2, is the vertical displacement of the free surface.The coupling between the fluid and the structure is expressed by equations (4) and (5). The first one means continuity of the normal velocity at the interface. The second one relates normal stresses of the solid on the interface with the pressure into the fluid and gravity effects if Tong hypothesis is used [5]. It must be noticed that Tong assumption is of crucial importance since it leads as this will be revealed later on to introduction of only symmetric operators.

In addition to the previous stated assumptions only the case of an axisymmetric reservoir under axisymmetric loading will be considered. It is assumed also that the structure is a thin shell for which

the Kirchhoff-Love assumption is valid. Provided that the angle α does not vary (this means that the axisymmetric shell has only straight elements as shown in figure 4 for a conical element having nodes i and j), the four generalized strain components are given in reference [6] by the following expressions in terms of the displacements of the middle shell surface and their derivatives:

$$\varepsilon_z = u^z{}_{,z} \tag{10}$$

$$\varepsilon_\theta = \frac{u^r \cos\alpha + u^z \sin\alpha}{r} \tag{11}$$

$$\kappa_z = -u^z{}_{,zz} \tag{12}$$

$$\kappa_\theta = \frac{-\sin\alpha}{r}\, u^r{}_{,z} \tag{13}$$

where $r = r(z)$ is the reference surface, u^r and u^z are the displacements in the local coordinates (r,z), κ_z and κ_θ are the local curvatures in the directions z and θ respectively. (R,Z) the global system of coordinates.

The four generalized stresses (obtained through an integration of the three-dimensional stresses σ with respect to the thickness of the shell) are related to the strains by the elasticity matrix D as follows:

$$\bar{\sigma} = D\bar{\varepsilon} \tag{14}$$

where

$$\bar{\sigma} = {}^t\left[N_z \quad N_\theta \quad M_z \quad M_\theta\right], \qquad \bar{\varepsilon} = {}^t\left[\varepsilon_z \quad \varepsilon_\theta \quad \kappa_z \quad \kappa_\theta\right]$$

and

$$D = \frac{Ee}{1-\upsilon^2}\begin{bmatrix} 1 & \upsilon & 0 & 0 \\ \upsilon & 1 & 0 & 0 \\ 0 & 0 & e^2/2 & \upsilon e^2/12 \\ 0 & 0 & \upsilon e^2/12 & e^2/12 \end{bmatrix}$$

for a homogeneous and isotropic shell material and a shell having uniform thickness e. E is the Young modulus and υ the Poisson coefficient.

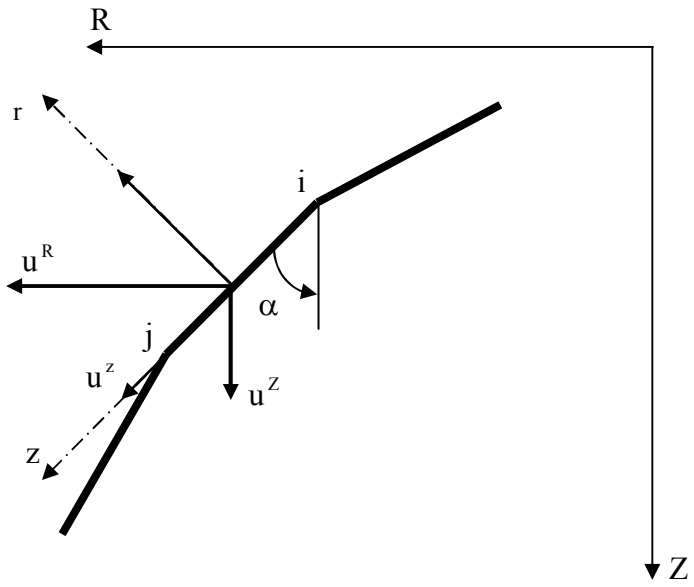

Figure 4: Geometry of the conical shell

When stationary solutions of the problem defined by equations (2) to (14) are searched under the spectral variational form, it can be shown that the equivalent problem, as it is demonstrated in reference [2] where an appropriate variational formulation along with Green formula have been used, is given by:

Find (φ, γ, v) defined on the time interval $[0, T]$ and taking their values in $H^1(\Omega_F) \times L^2(\Gamma_2) \times (H^1(\Omega_S))^2$ satisfying for every $(\psi, \xi, w) \in H^1(\Omega_F) \times L^2(\Gamma_2) \times (H^1(\Omega_S))^2$

$$\int_{\Gamma_2} \rho_F g \gamma \xi \, d\Gamma - p_0 \int_{\Gamma_2} \gamma \, d\Gamma - \omega^2 \int_{\Gamma_2} \rho_F \varphi \xi \, d\Gamma = 0 \tag{15}$$

$$\int_{\Omega_F} \rho_F \nabla\varphi.\nabla\psi \, d\Omega - \int_{\Gamma_1} \rho_F (v.n)\psi \, d\Gamma - \int_{\Gamma_2} \rho_F \gamma\psi \, d\Gamma = 0 \tag{16}$$

$$\int_{\Omega_S} \bar{\sigma}.\bar{\varepsilon} \, d\Omega + \int_{\Gamma_1} \rho_F g (k.n)(v.n)(w.n) \, d\Gamma - p_0 \int_{\Gamma_1} v.n \, d\Gamma - \omega^2 \int_{\Omega_S} \rho_S v.w \, d\Omega - \omega^2 \int_{\Gamma_1} \rho_F \varphi (w.n) \, d\Gamma = \int_{\Gamma_\sigma} f.w \, d\Gamma \tag{17}$$

2.3 Finite element discretization

Eqs. (15)-(17) as recalled above correspond to the weak form of the spectral problem. Solution can be found within the context of the finite element method. When two families of regular triangulations of Ω_F, Ω_S are considered, triangulations of Γ_1, Γ_2 and Γ_σ can be deduced such that the nodes

coincide. The unknowns of the variational spectral problem are approximated by those of the following discrete eigenvalue problem:

Find $\omega_h \geq 0$ and $(\varphi_h, \gamma_h, v_h) \in Y_h$ such that for every $(\psi_h, \xi_h, w_h) \in Y_h$ where $Y_h = L_h(\Omega_F) \times L_h(\Gamma_2) \times (L_h(\Omega_s))^2$ is the space of continuous piecewise functions on the regular triangulations of Ω_F and Ω_S with $w_h = 0$ on Γ_u:

$$\begin{aligned}\int_{\Omega_S} \overline{\sigma}(v_h).\overline{\varepsilon}(w_h)\,d\Omega + \int_{\Gamma_1} \rho_f g\,(k.n)(v_h.n)(w_h.n)\,d\Gamma + \int_{\Gamma_2} \rho_F g \gamma_h \xi_h\,d\Gamma = \\ \omega_h^2 \Big\{ \int_{\Omega_S} \rho_S\, v_h.w_h\,d\Omega + \int_{\Gamma_1} \rho_F\,(v_h.n)\psi_h\,d\Gamma + \int_{\Gamma_2} \rho_F\,\gamma_h \psi_h\,d\Gamma \\ - \int_{\Omega_F} \rho_F \nabla\varphi_h.\nabla\psi_h\,d\Omega + \int_{\Gamma_2} \rho_F \varphi_h w_h.n\,d\Gamma + \int_{\Gamma_2} \rho_F \varphi_h \xi_h\,d\Gamma \Big\} + \int_{\Gamma_\sigma} f.w_h\,d\Gamma\end{aligned} \tag{18}$$

and

$$\int_{\Gamma_1} v_h.n\,d\Gamma + \int_{\Gamma_2} \gamma_h\,d\Gamma = 0 \tag{19}$$

Let $\overline{v}$, $\overline{\varphi}$, $\overline{\gamma}$, $\overline{w}$, $\overline{\psi}$ and $\overline{\xi}$ denote the matrices of nodal components: v_h, φ_h, γ_h, w_h, ψ_h and ξ_h respectively. The matrices associated to the bilinear forms in the variational formulation are defined by:

${}^t\overline{w} K_S \overline{v} = \int_{\Omega_S} \overline{\sigma}(v_h).\overline{\varepsilon}(w_h)\,d\Omega$	stiffness matrix for the shell
${}^t\overline{w} M_S \overline{v} = \int_{\Omega_S} \rho_S v_h.w_h\,d\Omega$	mass matrix for the shell
${}^t\overline{\psi} F \overline{\varphi} = \int_{\Omega_F} \rho_F \nabla\varphi_h.\nabla\psi_h\,d\Omega$	mass matrix for the fluid
${}^t\overline{w} K_{\Gamma_1} \overline{v} = \int_{\Gamma_2} \rho_F g\,(k.n)(v_h.n)(w_h.n)\,d\Gamma$	associated with the gravity on the interface
${}^t\overline{\xi} K_{\Gamma_2} \gamma = \int_{\Gamma_2} \rho_F g \gamma_h \xi_h\,d\Gamma$	associated with the gravity on the free surface
${}^t\overline{\xi} B \overline{\varphi} = \int_{\Gamma_2} \rho_F \varphi_h \xi_h\,d\Gamma$	coupling between the fluid and its free surface
${}^t\overline{\psi} C \overline{v} = \int_{\Gamma_1} \rho_F \psi_h v_h.n\,d\Gamma$	coupling between fluid and solid variables

where ${}^t(\cdot)$ represents the transpose operation of a matrix.

The matrices associated to the linear forms in Eqs. (18) and (19) are defined by:

$${}^t c\overline{v} = \int_{\Gamma_1} v_h.n\,d\Gamma \;,\; {}^t b\overline{\gamma} = \int_{\Gamma_2} \gamma_h\,d\Gamma \text{ and } {}^t\overline{w}\,\overline{f} = \int_{\Gamma_\sigma} w_h.f\,d\Gamma\,.$$

In terms of these matrices, the discrete problem has the following form

$$\begin{bmatrix} K_S + K_{\Gamma_1} & 0 & 0 \\ 0 & K_{\Gamma_2} & 0 \\ 0 & 0 & 0 \end{bmatrix} \begin{bmatrix} \bar{v} \\ \bar{\gamma} \\ \bar{\varphi} \end{bmatrix} - \omega_h^2 \begin{bmatrix} M_S & 0 & {}^tC \\ 0 & 0 & {}^tB \\ C & B & -F \end{bmatrix} \begin{bmatrix} \bar{v} \\ \bar{\gamma} \\ \bar{\varphi} \end{bmatrix} = \begin{bmatrix} \bar{f} \\ 0 \\ 0 \end{bmatrix} \tag{20}$$

$${}^tc\bar{v} + {}^tb\bar{\gamma} = 0 \tag{21}$$

In case of free vibrations $\bar{f} = 0$, the fundamental following results were obtained in [7]:

- as h tends to zero, convergence of the solutions of Eqs. (20) and (21) to those of Eqs. (15) to (17) is demonstrated in case of three dimensional field equations of shell displacements;
- $\omega_h = 0$ is an eigenvalue of this problem with eigenspace $L_h(\Omega_F) \times \{0\} \times \{0\}$;
- apart from $\omega_h = 0$ the problem defined by Eq. (20) has a finite number of eigenvalues which are exactly those of the problem defined by Eqs. (20) and (21);
- Let consider the eigenmode of order m for which $\omega_h > 0$. If ω_h, v_h, φ_h, γ_h are solutions of Eq. (20), then they are solution of Eqs. (20) and (21) with

$$p_0 = p_m = \frac{\rho_F}{meas(\Gamma_2)} \int_{\Gamma_2} (g\gamma - \omega_h^2 \varphi)\, d\Gamma \tag{22}$$

System (20) can be rewritten under the compact form

$$(K - \omega_h^2 M)\, X = 0 \tag{23}$$

where ${}^tX = [\bar{v} \quad \bar{\gamma} \quad \bar{\varphi}]$.

General numerical methods for solving the eigenvalue problem defined by Eq. (22) such as those given in [8] can be used in order to extract the eigenvalues and eigenmodes. Here simple use of Calfem toolbox [9] under Matlab is made. Two kind of vibration modes can then be computed: low frequency sloshing modes and hydroelastic vibrations modes. The first ones correspond to the gravity waves on the surface of the liquid, the second ones are the vibration modes of the elastic reservoir modified by the interaction with the liquid.

The obtained modes depend on the actual gravity field g because K_{Γ_1} and K_{Γ_2} depend linearly on g. Analysis of the Pogo vibrations must be performed by taking also into account variations of the modes as function of liquid height in the propellant tank.

So, for a given reservoir geometry, fluid-structure material properties and acceleration of gravity, we have in general in accord with some triangulations of Ω_S and Ω_F: $\omega_m = \omega_m(H)$ and $X_m = X_m(H)$, where H is the height of liquid in the reservoir and m the order of the mode.

2.4 Frequency response model

So far, the undamped version of a modal model describing the various ways in which the reservoir partially filled with a liquid is capable of vibrating was developed. Assuming proportional damping yields that the modes of such damped coupled system are almost identical to those of the undamped

version of the model. Specifically, the mode shapes are identical and the natural frequencies are very similar to those of the simpler version of the model. The damped system will have the eigenvalues as follows:

$$\overline{\omega}^2 = \omega_m^2 (1 - \eta^2) \tag{24}$$

where $\overline{\omega}$ is the corrected angular frequency taking into account viscous damping. Fixing the damping factor η at less than 1% as stated in [1], yields that all the corrections to the frequencies are very small. So the undamped eigenmodes could be used here also in the presence of moderate viscous damping and we have an effectively undamped system.
However it is convenient to present the analysis of the structure's response as a response model [10]. That is the set of frequency response functions obtained as responses to unit-amplitude sinusoidal force applied to each point on the structure individually, and at every frequency within a specified range. The general element of the set of receptance frequency response functions is given by:

$$Y_{jk}(\omega) = \frac{\varphi_j}{f_k} = \sum_{m=1}^{M} \frac{A_{mjk}}{\omega_m^2 - \omega^2 + i\eta\omega_m^2} \tag{25}$$

where φ_j is the potential displacement response and f_k is the excitation force. $A_{mjk} = (\overline{X}_m)_j (\overline{X}_m)_k$ is the modal constant and $\overline{X}_m$ is the mass normalized version of the eigenvector of order m.
Equation (25) permits the calculation of one or more individual responses to an excitation of several simultaneous forces. Physically, the response of the system just at one of its natural frequencies is totally dominated by that mode and the other modes have very little influence [10]. In this way, each individual term of the second half of Eq. (25), could be considered as representing separately the system's response when the excitation frequency is in the vicinity of the related eigenvalue. So, for a small range of frequency in the vicinity of the natural frequency mode m, the frequency response function is effectively controlled by one of the terms in the series. Using Eq. (25), the receptance can be rewritten as

$$Y_{lk}(\omega) = \frac{A_{mlk}}{\omega_m^2 - \omega^2 + i\eta\omega_m^2} + B_{mlk} \tag{26}$$

where B_{mlk} is approximately independent from the frequency ω. This means that the combined effect of all the other modes can be represented as a constant term around the resonance frequency ω_m.
By using Eqs. (1), (22) and (26), the receptance in terms of pressure is obtained as

$$P_{lk}(\omega) = \frac{A_{mlk}\omega^2}{\omega_m^2 - \omega^2 + i\eta\omega_m^2} + B_{mlk}\omega^2 + p_m \tag{27}$$

2.5 Numerical results

The finite element method was applied to the computation of the vibration modes of an axisymmetric tank partially filled with a liquid. Data used in that analysis is listed in table 1.

Shell material density	$\rho_s = 7800\,\mathrm{Kg.m^{-3}}$
Young modulus	$E = 2.1\times10^{11}\,\mathrm{Pa}$
Poisson's coefficient	$\upsilon = 0.3$
Fluid density	$\rho_F = 1180\,\mathrm{Kg.m^{-3}}$
Shell length	$L = 7.4$ m
Shell radius	$R = 1.9$ m
Shell thickness (top plate and lateral)	$e_L = 4\times10^{-3}$ m
Shell thickness (bottom plate)	$e_R = 2.68\times10^{-2}$ m
Fluid height	$H = 3.7$ m

Table 1: Input data related to the tank geometry and material characteristics

Mode order	(1) Hz	(2) Hz	(3) Hz	(4) Hz	(5) Hz	(6) Hz	(7) Hz
1	0.2579	0.2539	0.2483	0.2452	0.7175	0.7103	0.7079
2	0.9929	0. 9719	0.7120	0.7094	1.0022	0. 9691	0.9579
3	2.2455	2.1715	0.9752	0.9622	1.2660	1.1822	1.1535
4	2.6264	2.3682	0.9901	0.9691	1.5402	1.3766	1.3201
5	4.0700	3.8789	1.1993	1.1648	1.8387	1.5638	1.4677
6	6.5225	6.0932	1.4131	1.3427	2.1665	1.7504	1.6017
7	9.6933	8.8404	1.6304	1.5069	2.5165	1.9406	1.7253
8	13.153	12.142	1.8580	1.6633	2.8570	2.1373	1.8406
9	13.683	12.911	2.0941	1.8159	3.1122	2.3427	1.9491

Table 2: Comparison of the first nine tank eigenfrequencies and convergence features
(1) FEM of Shell in vacuo (63 elements) (2) FEM of Shell in vacuo (123 elements)
(3) Hydroelastic FEM (184 elements) (4) Hydroelastic FEM (564 elements)
(5) Sloshing FEM (121 elements) (6) Sloshing FEM (441 elements)
(7) Sloshing analytic model

A finite element program was developed using Calfem toolbox in Matlab environment [9]. Table 2 gives, in case of a rigid tank, comparison of the first nine computed eigenfrequencies (columns 5 and 6) with the analytic ones (column 7) obtained from a formula presented in [11]. Convergence of the computed eigenmodes as function of the total number of elements is also considered. The obtained results assess both convergence and validate the program. Quantities underlined in table 2 are structural like frequencies. As a general remark coupling tends to decrease structural like frequencies while increasing sloshing like ones.

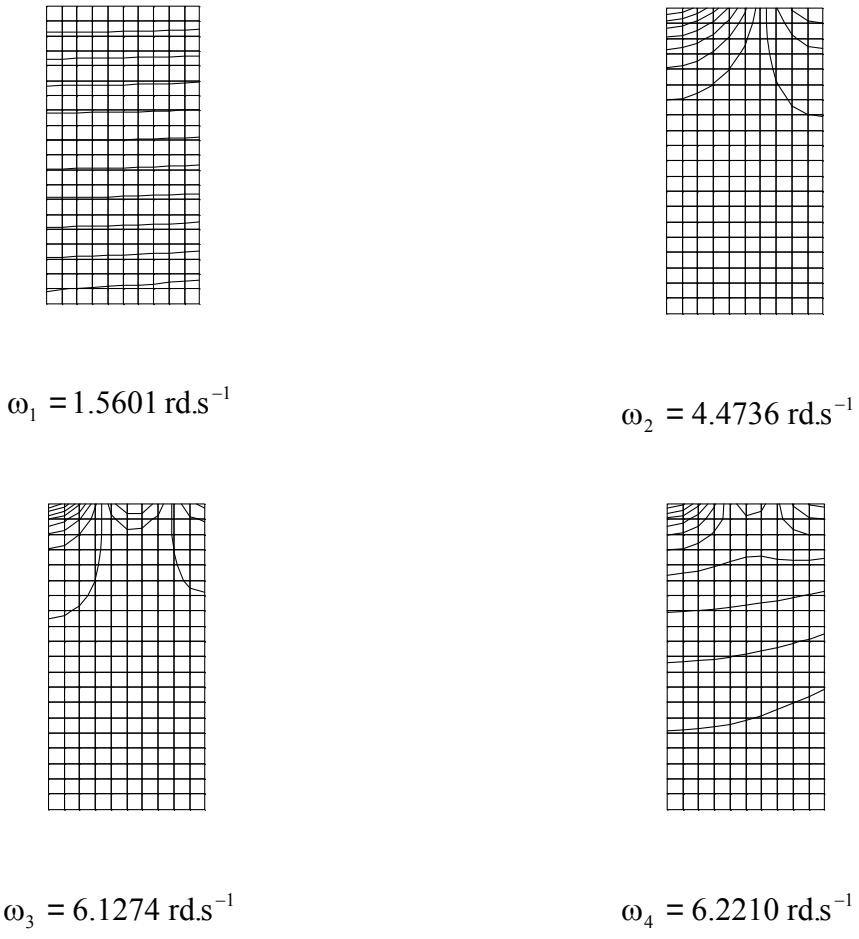

Figure 5: The first four coupled eigenmodes as pressure isolines

For a given coupled eigenmode where the eigenvalue $\omega_m > 0$, the pressure at any point is calculated from the values of the velocity potential φ at that point by using Eq. (1) where p_m is calculated by means of Eq.(22).

For $H = 3.7\ \text{m}$ and data listed in table 1, figure 5 represents the mode shapes as pressure isolines in the liquid for the four first coupled longitudinal eigenmodes for which convergence is within 5% interval.

Figure 6 gives the first nine eigenvalues as function of fluid height. Strong variations of frequencies are observed for small fluid depths. For $H > 0.8\ \text{m}$ all the nine frequencies tend to remain insensitive to the liquid height in the tank.

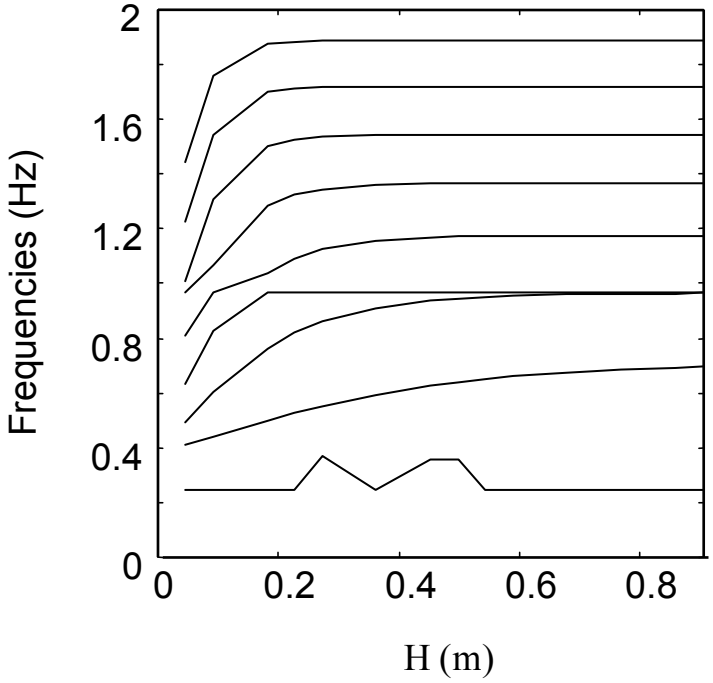

Figure 6: Frequency variations as function of liquid height

Table 3 gives the identified parameters A_m, B_m and p_m when the indices l and k are fixed such that the node where the force is applied coincides with the bottom edge of the tank and the pressure node is located on the tank axis of symmetry. Only the first three eigenmodes are considered. In general A_m, B_m decrease versus the mode order m, yielding that the most critical modes are the first ones.

Mode order	$\omega_m/(2\pi)$	$10^6 \times A_m$	$10^3 \times B_m$	p_m
1	0.2483	-0.13125	2.3404j	-29.410
2	0.7120	0.00907	0.27077j	-7.0310
3	0.9752	0.00058	0.14477j	-32.705

Table 3: Parameters of frequency response functions versus the mode order

3. MODELING THE ROCKET ENGINE

Propellant liquid reservoirs are equipped with engines for imparting propulsive thrust to the rocket. Ashley [12] has introduced an approach based on a one dimensional approximation of the problem. He has given the vehicle equations of motion and estimated thrust and fuel consumption when the steady-

flow energy equation, for the working fluid passing through the combustion chamber, is used. It is assumed also that the fluid is a pure, homogeneous substance and all the chemical reactions come to equilibrium between the inlet and outlet. This simple approximation treats the combustor as adding heat to the gas passing through, without changing the mass flow or the composition significantly. Thus, the ducted machine accelerates with an isentropic expansion a 1-D mass flow $\dot{m}_F$ from speed q_c in the undisturbed inlet to q_e at the nozzle exit. A typical nozzle has a converging-diverging bell-shaped form. We only consider here that a single monopropellant, like a perfect gas with constant R_c, is injected from the rocket reservoir to the combustion chamber. The constant R_c is proportional to the universal gas constant divided by the molecular weight of the combustion products. The propellants are brought to the desired pressure p_c by maintaining the entire tank at high pressure. After ignition the propellant is burned to chemical equilibrium, the pressure remains close to p_c, but temperature rises to a value θ_c which is fixed by the chemical reaction together with the specific heat of the products of combustion. The mixture is assumed to behave as a perfect gaz with an assigned average adiabatic constant γ_c. Upon finally neglecting pressure variation between the outlet exhaust and the surrounding ambient, the working expression for rocket thrust as derived in Ashley [12] simplifies to

$$T = h_c p_c \overline{S} \sqrt{1 - \left(\frac{p_e}{p_c}\right)^{\frac{\gamma_c - 1}{\gamma_c}}} + \frac{S_e}{\overline{S}\, p_c}(p_e - p_0) \tag{28}$$

where $\overline{S}$ is the nozzle throat area (section of minimum area), S_e the exhaust nozzle area, p_e is the exhaust pressure, p_0 the ambient pressure and the constant h_c is given in terms of the average coefficient γ_c as

$$h_c = \sqrt{\frac{2\gamma_c^2}{\gamma_c - 1}\left(\frac{2}{\gamma_c + 1}\right)^{\frac{\gamma_c + 1}{\gamma_c - 1}}} \tag{29}$$

The corresponding mass flow is

$$\dot{m}_f = p_c \overline{S} \sqrt{\frac{\gamma_c}{R_c \theta_c}\left(\frac{2}{\gamma_c + 1}\right)^{\frac{\gamma_c + 1}{\gamma_c - 1}}} = \overline{S} C^* \tag{30}$$

Let us now consider trajectories which reduce to a single vertical line passing through the center of a spherical nonrotating planet. We suppose that the rocket thrust is controlled by throttling the propellant flow without rotating the engine about gimbaled mounts. The controls are then T. The rocket specific impulse at sea level is defined [12] as

$$I_{sp} = \frac{T}{g \dot{m}_F} \tag{31}$$

where g is the gravity acceleration at sea level. Since T and $\dot{m}_F$ are constants, I_{sp} is also constant.
Table 4 gives thrusting characteristics for the four engines Viking 5C used in the first stage of Ariane IV. The propellant is N2O4/UDMH with the optimum oxidizer to fuel ratio: 2.61.

Specific Impulse	$I_{sp} = 248$ s
Combustion pressure	$p_c = 5.5$ MPa
Chamber temperature	$\theta_c = 3415$ K
Exhaust characteristic velocity	$C^* = 1720$ m.s^{-1}
Average specific density	$\rho_F = 1180$ Kg.m^3
Ratio of specific heats	$\gamma_c = 1.25$
Nozzle throat area	$\overline{S} = 0.7698$ m^2
Total propellant flow rate	$\dot{m}_F = 1116$ Kg.s^{-1}
Total thrust at sea level	$T = 2.7$ MN

Table 4: The engine characteristics

4. MODELING THE ENGINE FEEDLINE

The engine feedline is assumed here to be made from a straight cylindrical pipe having the uniform cross sectional area S. The pipe is made from a homogeneous, isotropic and linearly elastic material. The pipe structure containing the flowing liquid is assumed to be thin-walled. The radial compliance of the elastic pipe under the action of the liquid pressure is such that the modified wave speed of pressure surges propagation is c. The liquid is considered to behave as a compressible fluid column of length L.
It is assumed on the other hand that the junction between the inlet of the piping system and the reservoir has an impedance which can be approximated by that related to a small orifice radiating through a semi-infinite medium. The length of this transition zone which is very small is denoted L_1 in the following.
It is considered also that a pump is located at distance L_2 from the inlet zone of the pipe. The pump acts like a punctual source and its compliance is based on a linearization of the pressure rise Δp versus flow Δq at constant inlet pressure. Nonlinear phenomena such as cavitation process at pump inlets and non constant pump dynamic gain are neglected.
Within this framework of plane wave propagation approximation, small harmonic pressure and flow perturbations at each pipe downstream end are shown, [11], to be linked to those existing at the same pipe upstream end by the transfer matrices

$$\begin{bmatrix} q_d \\ p_d \end{bmatrix} = \begin{bmatrix} \cos(\alpha_\bullet) & \frac{\rho_f S}{jc}\sin(\alpha_\bullet) \\ -\frac{jc}{\rho_f S}\sin(\alpha_\bullet) & \cos(\alpha_\bullet) \end{bmatrix} \begin{bmatrix} q_u \\ p_u \end{bmatrix} \tag{32}$$

where $q_d = q_2, \Delta q$ or q_3, $q_u = q_1, q_2$ or Δq, $p_d = p_2, \Delta p$ or p_3 and $p_u = p_1, p_2$ or Δp. $q_\bullet$, respectively $p_\bullet$, is the flow, respectively the pressure at the considered pipe node. $\alpha_\bullet = \omega L_\bullet / c$, ω is the angular frequency and j the pure imaginary complex. Figure 7 presents the notations used.

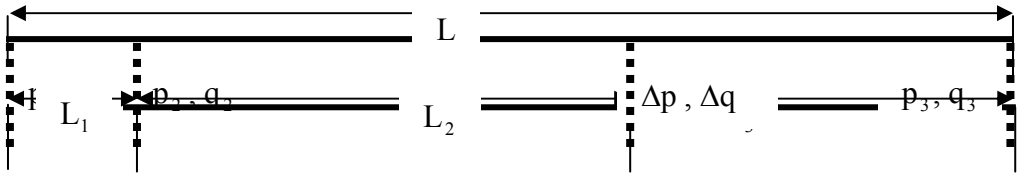

Figure 7: Geometry of the piping system

The impedance at the left end of the pipe is given by

$$p_1 = -j\gamma\omega q_1 = -\frac{8\omega j}{3\pi^{3/2} S^{1/2}} q_1 \tag{33}$$

That of the pump is constant and given by:

$$\Delta p = \lambda j \, \Delta q \tag{34}$$

Substituting now Eqs. (33) and (34) in the three system of equations resulting from (34), one obtains after performing some algebra

$$q_3 = \frac{j\rho_F S}{c\gamma\omega} \frac{\sin(\alpha_3 + \varphi_0)\left(\cos(\alpha_1) - \frac{\gamma S\omega}{c}\sin(\alpha_1)\right)}{\sin(\alpha_2 + \varphi_0)} p_1 \tag{35}$$

where $\varphi_0 = \tan^{-1}(\lambda S / c)$.

Eq. (35) shows that the resonance angular frequencies of the piping system are obtained by letting the denominator to vanish. These frequencies are given by:

$$\omega_n = \frac{c}{L_2}\left(\frac{\pi}{2} - \varphi_0 + n\pi\right) \tag{36}$$

where n is an integer.

Using Eq. (31), the thrust harmonic variation ΔT resulting from liquid flow perturbations is obtained as

$$\Delta T = g\, I_{sp} q_3 = G(\omega)\, p_1 \tag{37}$$

with

$$G(\omega) = \frac{j\rho_F g S I_{sp}}{c\gamma\omega} \frac{\sin(\alpha_3 + \varphi_0)\left(\cos(\alpha_1) - \frac{\gamma S \omega}{c}\sin(\alpha_1)\right)}{\sin(\alpha_2 + \varphi_0)} \tag{38}$$

In the limiting case where $\alpha_{k=1,2,3} \prec 1$ (i.e. $\omega \prec c / L_k$ for $k = 1,2,3$), a first order approximation of the acoustic feedline compliance is obtained as the following rational fraction

$$G(\omega) = \frac{j\rho_F g S I_{sp}}{c\gamma} \frac{\left(1 + \frac{L_3}{\lambda S}\omega\right)\left(1 - \frac{\gamma S L_1^2}{c^2}\omega^2\right)}{\omega\left(1 + \frac{L_2}{\lambda S}\omega\right)} \tag{39}$$

5. STABILITY ANALYSIS OF THE POGO LOOP

Pogo stability analyses should be preformed by considering the parameter uncertainties [1]. It should be performed at a sufficient number of flight time to establish completely the variation of system stability with time. Stability analyses should be performed by determining the closed-loop damping. The degree of stability in a given system mode is defined by a gain margin of structural damping required for neutral stability η_N, divided into the actual structural damping η [1]. For example when the actual structural damping equals 0.01, stability is stated when $\eta_N = 10^{-0.3}\ \eta \approx \eta / 2$.

However, in the context of the present study further simplifications are considered. First, analysis of the system stability by means of the closed-loop shown in the block diagram of figure 2 is considered when one structural mode is assumed to be predominant over all others. Second, we assume that $\eta_N < 0$. So, no positive damping must be present in the Pogo closed-loop near a given frequency of resonance for the coupled engine reservoir system.

According to definitions of receptance P in Eq. (27) and compliance G in Eq. (39), the block diagram shown in figure 2 becomes

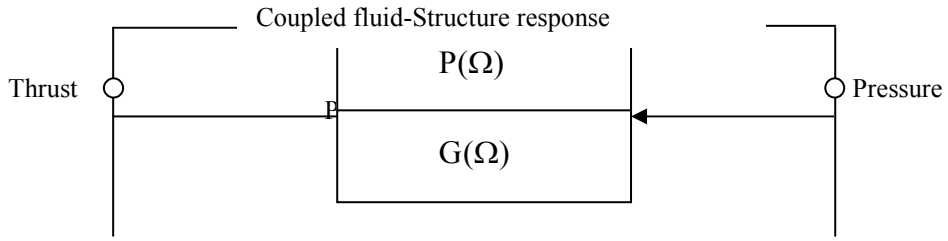

Figure 8: Block diagram of Pogo feedback process

For a given frequency Ω around the resonance frequency ω_m, the relative variation of pressure at the inlet of the piping system is equal to the relative variation of the global transfer function $H(\Omega)$ of the closed-loop. Thus,

$$\frac{\Delta p}{p} = \frac{\Delta H}{H} = \frac{1}{1+PG}\frac{\Delta P}{P} - \frac{PG}{1+PG}\frac{\Delta G}{G} \tag{40}$$

where as it is demonstrated in [17]

$$H(\Omega) = \frac{G(\Omega)}{1+P(\Omega)G(\Omega)} \tag{41}$$

It is the fact that expression $1+PG$ appears in denominators of the second half of Eq. (40) which is responsible for instability occurrence. This will be the case if at least one of the poles of H lies in the negative imaginary part of the complex plane.
The criterion of limit stability is therefore stated as follows: the charteristic equation

$$1 + P(\Omega)\, G(\Omega) = 0 \tag{42}$$

must have no root with negative imaginary part.
For given system parameters Eq. (42), can be solved in the general case by using Newton iterations in order to locate the complex roots.
Substituting Eqs. (25) and (39) into Eq. (42) yields the following polynomial equation

$$a_7\Omega^7 + a_6\Omega^6 + a_5\Omega^5 + a_4\Omega^4 + a_3\Omega^3 + a_2\Omega^2 + a_1\Omega + a_0 = 0 \tag{43}$$

with

$$a_7 = -j\chi abB_m$$
$$a_6 = -j\chi bB_m$$
$$a_5 = -\eta\chi abB_m\omega_m^2 + j(\chi aB_m - \chi abp_m + \chi abB_m\omega_m^2 + \chi abA_m)$$

$$a_4 = d - \eta\chi b B_m \omega_m^2 + j(\chi b A_m - \chi b p_m + \chi b B_m \omega_m^2 + \chi B_m)$$
$$a_3 = 1 + \eta\chi a B_m \omega_m^2 - \eta\chi a b p_m \omega_m^2 + j(\chi a p_m - \chi a A_m - \chi a B_m \omega_m^2 + \chi a b p_m \omega_m^2)$$
$$a_2 = -d\omega_m^2 + \eta\chi B_m \omega_m^2 - \eta\chi b p_m \omega_m^2 + j(\chi p_m - \chi A_m + \chi b p_m \omega_m^2 - \chi B_m \omega_m^2 - \eta d \omega_m^2)$$
$$a_1 = -\omega_m^2 + \eta\chi a p_m \omega_m^2 + j(-\eta\omega_m^2 - \chi a p_m \omega_m^2)$$
$$a_0 = \eta\chi p_m \omega_m^2 - j\chi p_m \omega_m^2$$

where $a = \frac{L_3}{\lambda S}$, $b = \frac{\gamma S L_1^2}{c^2}$, $d = \frac{L_2}{\lambda S}$ and $\chi = \frac{\rho_F g S I_{sp}}{\gamma c}$.

Solution of Eq. (43) can be performed by using Matlab and the stability criterion verified. One must also verify that approximations $\alpha_{k=1,2,3} \prec 1$ used to transform Eq. (38) into Eq. (39) are valid. Then only the roots of Eq. (43) having the smallest real parts are of interest.

6. NUMERICAL RESULTS

To achieve parametric study of Pogo stability, the feedline parameters data listed in table 5 is used. The pump compliance is kept variable. Parameters ω_m, A_m, B_m and p_m are fixed by choosing a longitudinal mode among the three first ones given in table 3 for which convergence is likely reached. Besides, only the particular case $H = 3.7$ m is considered. But it will be sufficient to demonstrate instability.

Feedline cross sectional area	$S = 0.0733\ m^2$
Length L_1	$L_1 = 0.6$ m
Length L_2	$L_2 = 25$ m
Length L_3	$L_3 = 1$ m
Water hammer wave speed	$c = 1200\ m/s$
Proportional damping ratio	$\eta = 0.01$

Table 5: The feedline parameters

Figure 9-a, 9-b and 9-c show the imaginary and real parts versus parameter λ for the first three modes. Pogo instability is observed in the present system when $-20 < \lambda < 0$ for the first mode and when $\lambda < 0$ for the two others.

An extensive parametric study has also shown that it is hard to obtain a Pogo stable system. This may explain why all the Ariane engines are systematically equipped with Pogo corrective devices.

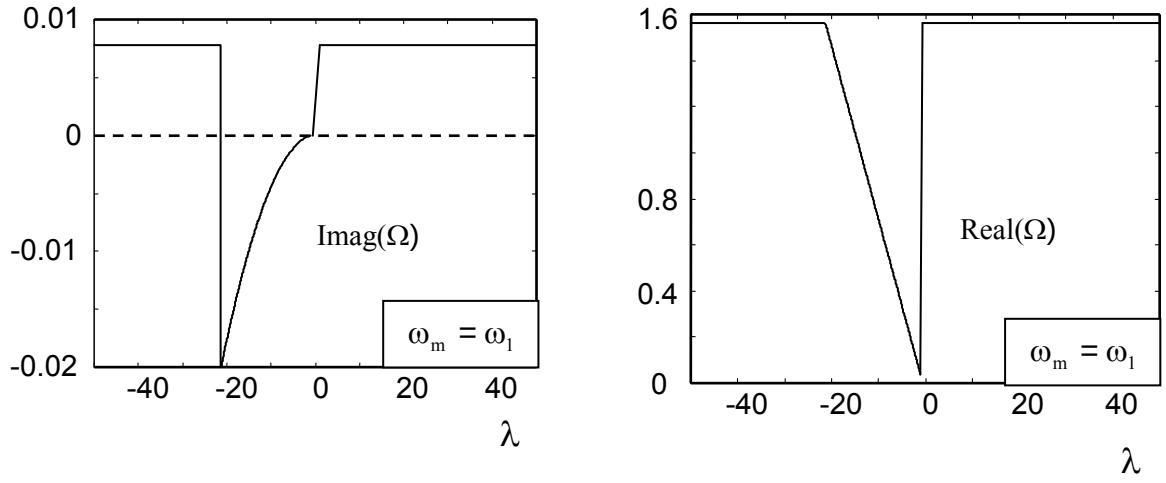

Figure 9-a: Stability diagrams as function of the pump impedance for ω_1

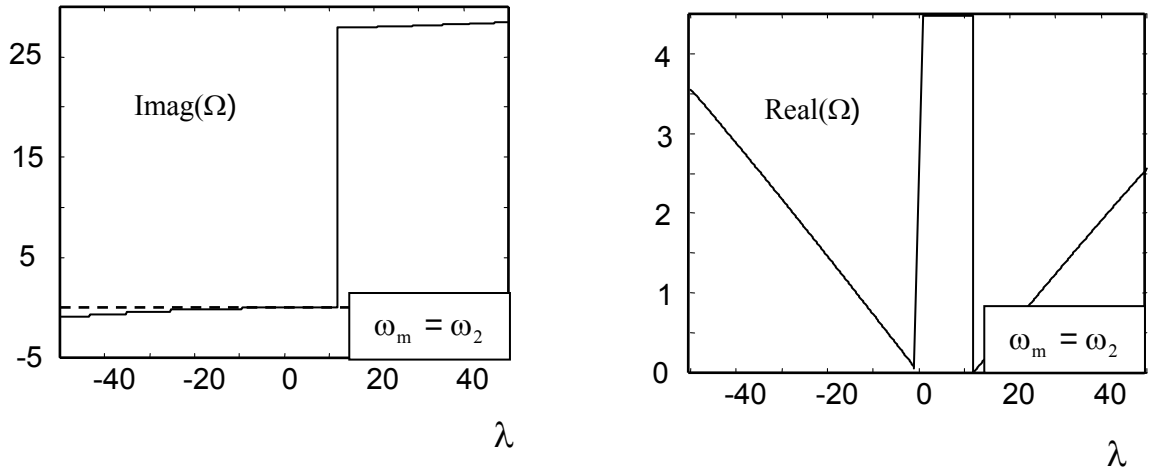

Figure 9-b: Stability diagrams as function of the pump impedance for ω_2

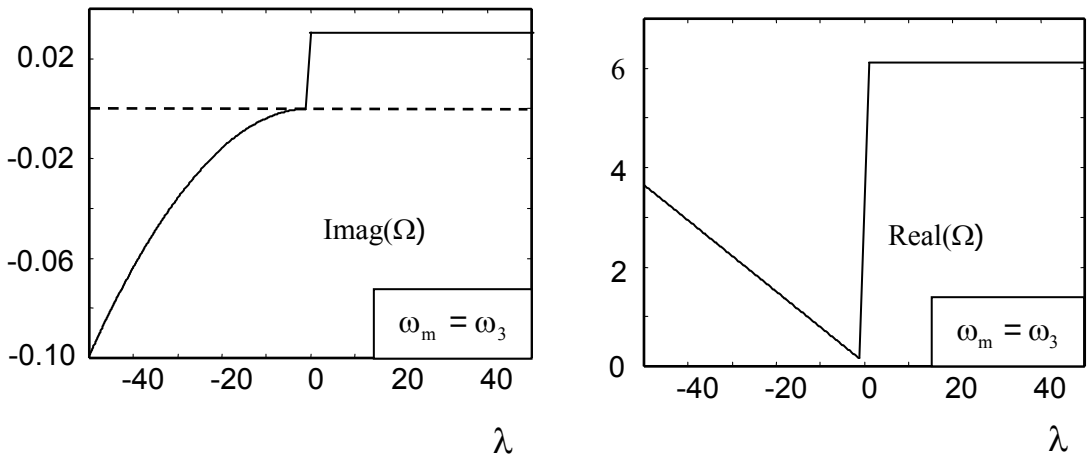

Figure 9-c: Stability diagrams as function of the pump impedance for ω_3

7. CONCLUSIONS

A theoretical modeling of Pogo instability occurring in rockets was proposed. The model uses frequency response functions obtained from the coupled modes of the partially filled tank incorporating both hydroelastic and gravity effects. It uses also the transfer function of the secondary system and the engine which was obtained by assuming plane wave approximation and static relation between the thrust and the propellant rate flow.
Under the assumption of small frequency range a characteristic equation of order seven was obtained. This equation is the numerator of the gain function associated with the closed loop having as the mean branch the fluid-structure response function between the engine bolts and the upstream end of the feedline, and as the feedback branch the transfer function of the piping system feeding the engine.
Solution of this equation enables analysis of Pogo stability. For a given frequency which is in the vicinity of a longitudinal eigenfrequency of the rocket, the system is instable if the imaginary part of the root having the smallest positive real part is negative.
Considering a case study the model has shown that Pogo instability could occur for some selected impedances of the pump feeding the engine.
Through extensive parametric studies it was found that a rocket is more likely to be Pogo sensitive. This explains why anti Pogo corrective devices are widely used in the prevention of this special kind of instabilities.

8. REFERENCES

1. Rubin S. and Jones G.W., Prevention of coupled structure-propulsion instability (Pogo), Space Vehicle Design Criteria (Structures), NASA SP-8055, 1970.
2. Valid R., Ohayon R., Berger H., Le calcul des réservoirs élastiques partiellement remplis de liquides, pour la prévision de l'effet Pogo, La Recherche Aérospatiale, N.6, 367-379, 1974.
3. Morand H.J.P., Ohayon R., Interactions fluides-structures, Recherche en Mathématiques Appliquées 23, Masson, Paris, 1992.

4. A. Bermúdez, R. Rodríguez, Finite element analysis of sloshing and hydroelastic vibrations under gravity, RAIRO – Mathematical Modelling and Numerical Analysis, 33, 305-327, 1999.
5. Tong P., Liquid sloshing in an elastic container, ASQSR 66-0943, California Institute of Technology, Pasadena, CA, 1960.
6. Zienkiwicz O.C., The finite element method in engineering science, McGraw-Hill, New York, 1971.
7. A. Bermúdez, R. Rodríguez, D. Santamarina, A finite element solution of an added mass formulation for coupled fluid-solid vibrations, Numerische Mathematik, 87, 201-227, 2000.
8. M. Mellado, R. Rodríguez. Efficient solution of fluid-structure vibration problems. Applied Numerical Mathematics, 36, 389-400, 2001.
9. Calfem: a finite element toolbox to Matlab, version 3.2, Division of Structural Mechanics LTH, Lund University, Sweden.
10. Ewins D.J., Modal testing : theory and practice, Research Studies Press Ltd., John Wiley and Sons Inc., New York, 1986.
11. Gibert R.J., Vibrations des structures, Collection Eyrolles, France, 1988.
12. Ashley H., Engineering analysis of flight vehicles, Dover Publications Inc., New York, 1974.
15. Bermúdez A., Rodríguez R., Santamarina D., Finite element approximation of a displacement formulation for time-domain elastoacoustic vibrations, Journal of Computational an Applied Mathematics, 152, 17-34, 2003.
16. Bermúdez A., Rodríguez R., Santamarina D. Finite element computation of sloshing modes in containers with elastic baffle plates. International Journal for Numerical Methods in Engineering, 56, 447-467, 2003.
17. Dieulsaint E., Royer D. Automatique appliquée: 1-Systèmes linéaires de commande à signaux analogiques. Masson, Paris, 1987.